Macromolecules
Cite This: Macromolecules XXXX, XXX, XXX−XXX
Article
pubs.acs.org/Macromolecules

Nanopatterning of Solvent between Apposing Planar Brushes under Pressure

Claudio Pastorino,[†,‡] Yongwook Kim,[§] Sergiy Minko,[§] and Marcus Müller*[,∥]

[†]Departamento de Física de la Materia Condensada, Centro Atómico Constituyentes, CNEA, Av. Gral. Paz 1499, 1650 Pcia, Buenos Aires, Argentina

[‡]CONICET, Godoy Cruz 2290, C1425FQB Buenos Aires, Argentina

[§]Nanostructured Materials Lab, University of Georgia, Athens, Georgia 30602, United States

[∥]Institut für Theoretische Physik, Georg-August Universität Göttingen, 37077 Göttingen, Germany

ABSTRACT: Using computer simulation of a coarse-grained, bead−spring model as well as scanning-probe microscopy of polytBA brushes in ethanol, we demonstrate that upon compression a poor solvent between two apposing polymer brushes does not remain a uniform thin film but, instead, forms a lateral, nanoscopic structure. The characteristic lateral length scale of the solvent domains scales with the brush height that, in turn, can be controlled by the grafting density, molecular weight, or pressure. These findings are rationalized in terms of geometric considerations, accounting for the interfacial free energy between the solvent and the brush and the spatial arrangement of the grafted chains. The phenomenon offers a general strategy to laterally structure confined fluids.

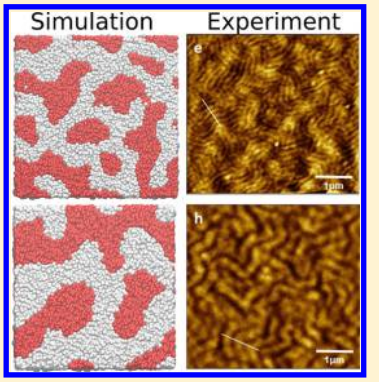

INTRODUCTION

Polymer brushes consist of macromolecules that are irreversibly grafted to the surface. They find widespread applications as resistant and versatile coatings that are employed to tailor surface properties such as wettability, adhesion, and friction.[1−6] Immersed in a good solvent, the behavior of a swollen polymer brush is dictated by an interplay between repulsive interactions among the brush segments and the entropy loss as the macromolecules stretch away from the grafting surface.[7−12] Under moderately poor solvent conditions and high grafting densities, however, the brush collapses into a dense uniform layer.[13,14] The density, ρ_0, of the film is comparable to the density of the nongrafted polymer liquid and the polymer brush is separated from the solvent by a narrow interface. In the case of very poor solvent or low grafting density, polymer dimples or pinned micelles are formed.[15−22] These lateral structures are composed of globular cores and extended legs connecting the core with the grafting surface. Also, the formation of these pinned micelles between apposed surfaces has been considered as a means to tailor the interaction between surfaces or brush-coated colloids.[18,19]

In the following we consider a polymer brush in a moderately poor solvent such that the brush collapses into a uniform layer in coarse-grained simulations and experiments. Upon bringing two brush-coated surfaces into apposition (cf. Figure 1), however, we observe that the squeezed solvent layer laterally breaks up into threads. We explore the dependence of this lateral patterning of the solvent on the nanoscale as a function of the grafting density and molecular weight of the brush and rationalize our observation by a simple, geometric model.

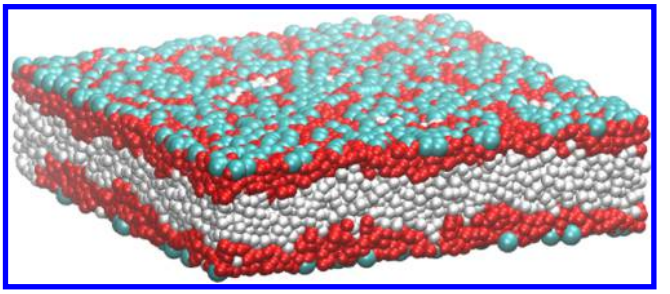

Figure 1. Snapshot of a solvent film confined between two brush-coated surfaces. Solvent particles are presented in gray, coarse-grained polymer segments are shown in red, except for the grafted ends that are depicted in light blue. The film thickness is $D = 16\sigma$, and the brushes are formed by 16-bead polymer chains.

Our paper is arranged as follows: In the next two sections, we describe the simulation model and techniques as well as the experimental system, respectively. Subsequently, we investigate the lateral and perpendicular structure of the apposed brush system. The paper closes with a brief discussion and an outlook.

Received: April 24, 2018
Revised: July 20, 2018

DOI: 10.1021/acs.macromol.8b00865
Macromolecules XXXX, XXX, XXX−XXX

SIMULATION TECHNIQUE

To study the universal behavior of the brush−solvent system, we employ a coarse-grained polymer model. Coarse-grained polymer segments[23] and solvent particles interact via a truncated and shifted, purely repulsive Lennard-Jones potential

$$U(r) = U_{LJ}(r) - U_{LJ}(r_c) \quad \text{for } r < r_c \tag{1}$$

with

$$U_{LJ}(r) = 4\varepsilon_{\alpha\beta}\left[\left(\frac{\sigma_{\alpha\beta}}{r}\right)^{12} - \left(\frac{\sigma_{\alpha\beta}}{r}\right)^{6}\right] \tag{2}$$

where the Greek indexes denote the different particle types, polymer and solvent; r is the distance between particles, and $r_c = \sqrt[6]{2}\sigma_{\alpha\beta}$ quantifies the cutoff radius, beyond which particles do not interact. The interaction range of particles of the same type is identical and defines the length scale, $\sigma_{\alpha\alpha} = \sigma$. The range of the repulsion between polymer and solvent is increased to $\sigma_{ps} = 1.2\sigma$. This nonadditivity gives rise to an enhanced repulsion between polymer and solvent;[24] i.e., the brush is immersed in a poor solvent. ε sets the energy scale of the pairwise interactions and we set $k_BT = 1.68\varepsilon$.

The polymer chains of the brush are composed of $N_b = 10$, 16, 32, or 64 coarse-grained segments that are connected by a finitely extensible nonlinear elastic (FENE) potential

$$U_{FENE} = -\frac{1}{2}kR_0^2 \ln\left[1 - \left(\frac{r}{R_0}\right)^2\right] \quad \text{for } r < R_0 \tag{3}$$

with $k = 30\varepsilon/\sigma^2$ and $R_0 = 1.5\sigma$.[23] Under these conditions the statistical segment length is $b \equiv \frac{\langle \mathbf{R}_e^2 \rangle}{N-1} \approx 1.27\sigma$[25] where $R_e^2 \equiv \langle \mathbf{R}_e^2 \rangle$ denotes the mean-squared end-to-end distance of a polymer.

We consider a thin film confined between two impenetrable surfaces that are spaced a distance $8\sigma \le D \le 40\sigma$, apart along the $\hat{z}$-direction. The confining surfaces are purely repulsive and interact with all particles via

$$U_{surf}(z) = A_w\left[\left(\frac{\sigma_w}{\Delta z}\right)^9 - \left(\frac{\sigma_w}{\Delta z}\right)^3\right] \quad \text{for } \Delta z < \sqrt[6]{3}\sigma \tag{4}$$

with $A_w = 2\varepsilon$ and $\sigma_w = 1\sigma$. $\Delta z = z$ or $D - z$ denotes the distance from the surfaces. One terminal segment of each brush chain is irreversibly grafted at a random, lateral position onto the confining surfaces.

Periodic boundary conditions are applied in the two lateral directions, $\hat{x}$ and $\hat{y}$, of length $L = L_x = L_y = 60\sigma$. The surface area A and the number of polymers n_{brush} dictate the grafting density, $\sigma_g = \frac{n_{brush}}{2A} = 0.167/\sigma^2$; i.e., the system is composed of 2×600 polymers.

Our molecular dynamics simulation use the velocity-Verlet algorithm in conjunction with a dissipative particle dynamics (DPD) thermostat.[26−28] The pairwise forces consist of a conservative force, $\mathbf{F}_C$, derived from the interactions, a random force, $\mathbf{F}_R = \zeta\omega_R(r)\eta\hat{r}$, and a dissipative force, $\mathbf{F}_D = -\gamma\omega D(r)(\hat{\mathbf{r}}\cdot\mathbf{v})\hat{\mathbf{r}}$ with $\hat{r} = \mathbf{r}/|\mathbf{r}|$ and η being a random number with zero average and unit variance. $\gamma = 0.5\varepsilon\tau/\sigma^2$ quantifies the friction, and $\mathbf{v}$ is the difference of velocities of the particles of the considered pair. The choice $\zeta^2 = 2k_BT\gamma$ and $\omega_R^2 = \omega_D = (1 - r/r_c)^2$ with $r_c = 2\sqrt[6]{2}\sigma$ fulfills the fluctuation−dissipation theorem.

The stochastic equations of motion were integrated with a time step of $\delta t = 2 \times 10^{-3}\tau$, with $\tau = \sigma\sqrt{m/\varepsilon}$ and particle mass $m = 1$. A typical simulation is composed of 2×10^7 integration steps or $10^3\tau$, including 3×10^6 steps for equilibration.

EXPERIMENTAL SECTION

Materials. Silicon wafers were purchased from Semiconductor Processing (Boston, MA). Polydimethylsiloxane (PDMS) films were prepared using Sylgard-184 Silicone Elastomer kit (Dow Corning Co., USA). The chemicals (3-aminopropyl)triethoxysilane (APS), α-bromoisobutyryl bromide (BIBB), trimethylamine (TEA), anhydrous dichloromethane (Aldrich), copper bromide ($CuBr_2$), *N,N,N,N,N*-pentamethyldiethylenetriamine (PMDTA), ethyl-2-bromoisobutyrate (EBiB), and ascorbic acid (ASCO) were purchased from Millipore-Sigma and used as received. *tert*-Butyl acrylate (tBA, Millipore-Sigma) was used after a purification: tBA was filtered using a neutral aluminum oxide column to remove the inhibitor prior to polymerization.

Preparation of Samples. *PDMS-Coated Wafers.* PDMS solutions were prepared by dissolving 3 wt % of the ingredients of the Sylgard-184 kit (monomer to curing agent ratio 10:1) in hexane. The solution was spin-coated at 6000 rpm on the silicon wafer substrates for 150 s. Afterward, the films were annealed at 85 °C for 1 h. The thickness of the PDMS film is 160 ± 10 nm as evaluated with scanning probe microscopy (SPM) using samples with scratched PDMS films (the scratches were made down to the silica layer on the Si-wafer surface). The PDMS-coated wafers were treated with an air plasma (1 MPa) to oxidize the surface of the PDMS film and form a thin film of silica on the top of the PDMS film.

Grafting of PolytBA from PDMS-Coated Wafers. The plasma-treated PDMS coated wafers were incubated in a 1% ethanol solution of APS overnight to functionalize the surface of the film with amino-functional groups and prevent a reconstruction of the surface. Afterward, the samples were washed with ethanol and incubated for 2 h in 40 mL of anhydrous CH_2Cl_2 with 1% BIBB and 2% TEA to immobilize the initiator of polymerization. This was followed by rinsing of the wafer with CH_2Cl_2 and ethanol. tBA brushes were grafted from the functionalized wafers using activator generated by electron transfer−atomic transfer radical polymerization (AGET-ATRP) as described elsewhere.[29] The reactants for grafting: 280 μL of 0.1 M $CuBr_2$, 9 μL of 0.68 M EBiB, and 280 μL of 0.5 *m* PMDTA were added to 30% ethanol solution (for PtBA100 and PtBA190 samples) or 10% ethanol solution (for PtBA40 sample) of tBA and dissolved oxygen was removed by purging the solution with argon gas for 20 min. Then, 450 μL of ASCO (0.176 g/mL) was injected into the polymerization reactor slowly, and this was followed by degassing with argon. The polymerization was allowed to proceed for 30 min, 1 h, and 2 h at a temperature of 60 °C. By opening the cap and cooling the reactor, the reaction was stopped. The samples were rinsed with ethanol three times and dried in the air. Three samples were synthesized denoted as PtBA40, PtBA100, and PtBA190 where the digits show the brush thickness in nm (Table 1). Molecular weight (MW) and polydispersity index (PDI) for the brush samples were estimated with gel permeation chromatography (chloroform mobile phase) using polymer samples collected from the bulk solutions. Poly(tBA) was precipitated in methanol containing 15% water and dried at the room temperature. SPM was used to estimate thickness of

Table 1. Characteristics of PolytBA Brushes

	MW (g/mol)				
sample	M_n	M_w	thickness (±10 nm)	grafting density (±0.2 chains/nm²)	PDI
PtBA40	26800	42000	40	0.6	1.55
PtBA100	50000	99000	100	0.6	1.97
PtBA190	55200	102000	190	1.1	1.84

DOI: 10.1021/acs.macromol.8b00865
Macromolecules XXXX, XXX, XXX−XXX

grafted polytBA brushes using scratches on the film surface (down to the silica substrate). The brush thickness was calculated as a difference of the scratch depth minus the thickness of the PDMS film previously estimated using the same scratch depth method as described above.

Formation of Pressure Induced Patterns in Poor Solvent. Two 1 cm × 1 cm samples with the same grafted polytBA brush were immersed in an ethanol bath and pressed face-to-face with a force of 10 N overnight. Afterward, the samples were detached and rapidly dried in the air at room temperature and left for at least 30 min prior to examination of surface morphology with SPM. The SPM studies were conducted with a Dimension Icon microscope (Bruker Co.) to visualize the brush morphology using the tapping mode with DPN-S probe (Bruker, a silicon nitride tip with a diameter of 20 nm and a spring constant of 0.35 N/m) at room temperature.

RESULTS

Simulations. *Dependence on the Brush Separation, D.* A snapshot of the brush-covered slit channel for chain length $N_b = 16$ and $D = 16\sigma$ is presented in Figure 1. From this side view, we observe a "sandwich" configuration with a brush−solvent−brush structure and a laterally uniform solvent layer around the midplane of the system, $z = D/2$.

Laterally averaged number-density profiles of polymer and solvent particles are shown in Figure 2a. As expected, the brush

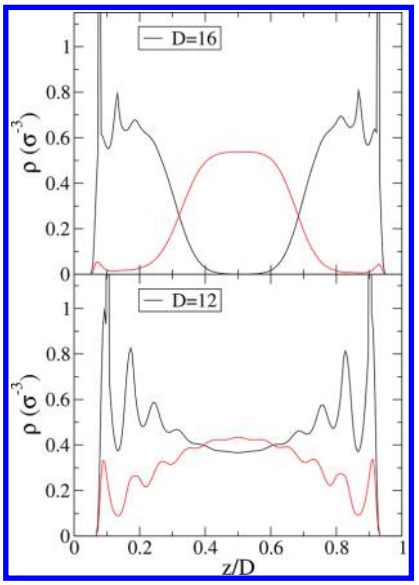

Figure 2. Density profile of polymer (black) and solvent (red) particles across the film for thickness (a) $D = 16\sigma$ and (b) $D = 12\sigma$. In the former case (a) the solvent forms a homogeneous layer in the middle of the film, whereas it is laterally structured in the latter case (see also panels a and b of Figure 3). The ordinate axis, z/D, is scaled with the film thickness, D.

is collapsed into a dense layer that is separated by a rather narrow interface from the incompatible solvent. From the profiles we observe that there is still a small amount of solvent inside the brush, corresponding to local fluctuations of the composition that correlate with locations of low grafting density. Because the brush thickness, h_b, and the segment size, σ, are not well separated, we observe rather pronounced, liquid-like layering effects not only in the ultimate vicinity of the hard, impenetrable surface but inside the brush.[25,30,31] Nevertheless, we can roughly estimate the brush thickness by $n_b \approx N_b\sigma_g/\rho_0 \approx 4.45\sigma = 0.28D$, where $\rho_0 \approx 0.6/\sigma^3$ denotes the density of the solvent. The small amount of solvent inside the brush and the packing effects slightly modify this simple estimate (cf. Figure 2a), but the brush height h_b does not exceed the polymers end-to-end distance, $R_e \approx 4.9\sigma$; i.e., the brush is not stretched away from the grafting surface.

In the following, we compress the film at constant number of particles; i.e., as we reduce the film thickness D, the density and pressure increase. Already upon reducing the distance between the brushes to $D = 12\sigma$, we observe that the laterally averaged density profiles qualitatively change—most notably, polymer *and* solvent particles are present at the center of the film.

Figure 3 presents lateral cross-cuts of the morphology along the central plane of the system at $z = D/2$. Whereas for $D = 16\sigma$ the system is laterally homogeneous, we observe lateral structure formation for the smaller thicknesses, $D/\sigma = 12$, 10, and 8. Rather than uniformly thinning the solvent layer, the confined solvent condenses into a fingerprint-like pattern of threads with a characteristic width and thereby allows the apposing brushes to make an energetically favorable contact outside the solvent threads. The width of the solvent threads slightly decreases upon reducing the film thickness from $D = 12\sigma$ to $D = 10\sigma$. As we reduce D further, the number density of Lennard-Jones particles exceeds unity and we observe a crystallization of the monomeric solvent.

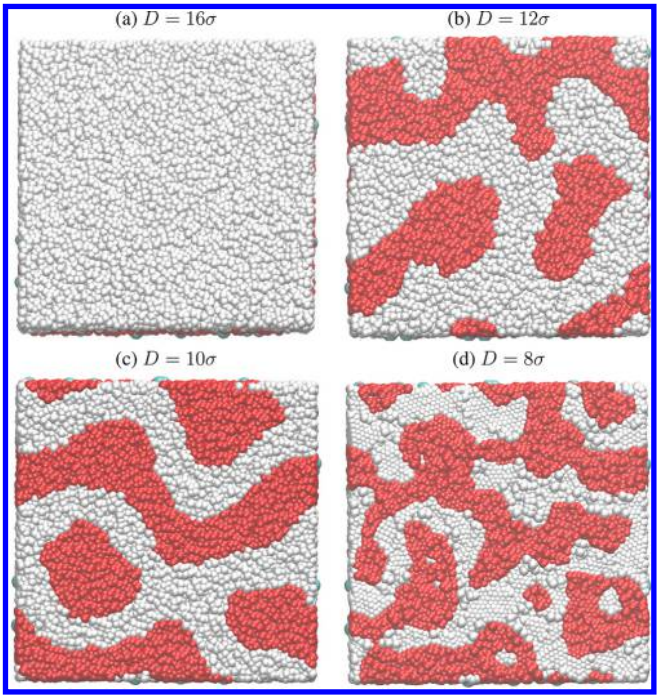

Figure 3. Snapshots of the morphology in the middle of the thin film at fixed chain length, $N_b = 16$, as a function of film thickness, D. The image shows a cut across the center plane of the film at $z = D/2$. The coloring of solvent and polymer breads is the same as in Figure 1. From panels a−d, the film thickness, D, decreases as indicated in the key.

This lateral structure formation also rationalizes the averaged density profiles in Figure 2b; rather than a mixing between polymer and solvent, the profiles arise from a lateral microphase separation. This transition of morphology between a laterally uniform sandwich structure and a lateral microphase separation between grafted polymer and solvent upon confinement is the central topic of this work.

DOI: 10.1021/acs.macromol.8b00865
Macromolecules XXXX, XXX, XXX−XXX

Dependence on the Length, N_b, of the Brush Chains. Whereas the pressure-induced decrease in the film thickness, D, demonstrates the basic phenomena, the increase of density inside the film complicates the interpretation. As D decreases, the incompatibility between solvent and polymer and the concomitant surface tension, γ, of the polymer−solvent interface increases and even the polymer conformations in the bulk slightly depend on density.

In a second set of simulations, we vary the chain length of the brush, N_b = 64, 32, 16, and 10 but leave the grafting density unaltered. We fix the fraction of solvent particles, $\bar{\phi} \equiv \frac{N_{solv}}{N_b n_{brush} + N_{solv}} = 0.235$, to observe a similar morphology and approximately adjusted the film thickness, D, for each N_b, so that the density at the center of the film does not vary with N_b. The latter condition corresponds to a situation where the solvent can laterally drain out of the confined region between the apposed brushes.

Also in this case we observe lateral microphase separation between the grafted polymer and solvent as presented in Figure 4. The characteristic size of the microphase-separated

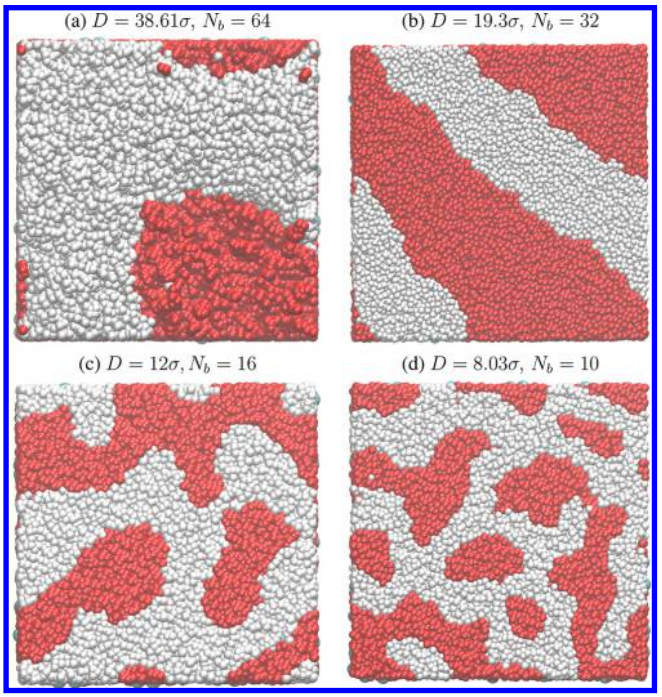

Figure 4. Morphology in the middle of the film as a function of the length, N_b, of the brush molecules. The film thickness, D, given in the key, is adjusted such that the density in the middle of the film remains unaltered. The coloring of solvent and polymer breads is the same as in Figure 1.

solvent threads exhibit a significant dependence on N_b. To quantify the lateral length scale, we have graphically analyzed six configurations for each N_b. The results for the width, w, as a function of N_b are presented in Figure 5. The data are compatible with a linear increase, $w \approx 0.42\sigma N_b$, as indicated by the dashed line.

Comparing this value to the brush height, $h_b = \sigma_g N_b/\rho_0 \approx 0.23\sigma N_b$, we observe that the width of the solvent domains is approximately $w \approx 1.83 h_b$. This simple relation is further supported by the experiments and corroborated by a geometric model that are presented in the following sections.

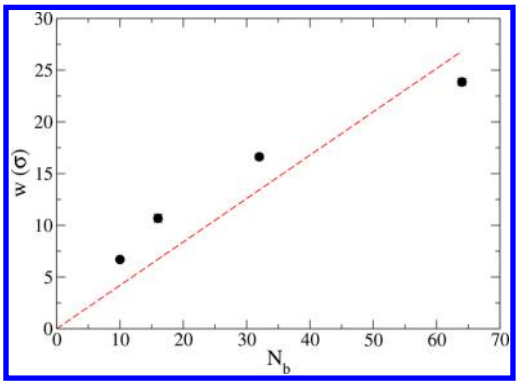

Figure 5. Width, w, of the solvent thread as a function of polymer size, N_b. The dashed line shows a linear fit.

The simulations allow for a quantitative description of the polymer and solvent distributions. In analogy to the fingerprint morphology of block copolymer thin films, we expect that the solvent threads will ideally form linear, one-dimensional objects similar to Figure 4b. For this system, N_b = 32 and $D = 19.3\sigma$, panels a and b of Figure 6 present the number density of polymer and solvent particles as a function of the two lateral coordinates, x and y, averaged over $0 < z < D/2$. In this two-dimensional top-down view, one can clearly identify the one-dimensional solvent threads, as dark and bright regions in panels a and b, respectively. The bright spots in panel a mark the positions of the immobile grafting points. Because of the random grafting, the local density of grafting points fluctuates, and the solvent thread is preferentially located on top of local depressions of grafting density and the thread is also slightly wider. This correlation between the morphology and quenched fluctuations of the grafting points may potentially explain why we do not observe lateral structures with long-range order.[22]

Panels c and d of Figure 6 show the two-dimensional profile of polymer and solvent density, averaged along the axis of the solvent thread, using a rotated and cropped sample. One can clearly observe the ellipsoidal cross section of the solvent thread, although fluctuations of the centerline of the thread may somewhat broaden the profile. The two-dimensional cross section of the liquid thread indicates that the solvent reaches almost up to the grafting surfaces at $z = 0$ and $z = D$. This information about the geometry of the solvent thread is subsequently employed in the geometric model.

Depending on the volume fraction, $\bar{\phi}$, of the solvent, the morphology of the solvent domains may change. In the previous case, the solvent density was $\rho_s = 0.17\sigma^{-3}$, corresponding to a solvent fraction of $\bar{\phi} = 0.235$, and we observed a fingerprint-like pattern of solvent threads.

Figure 7 shows the morphology when the solvent fraction is reduced to a value of $\bar{\phi} = 0.091$ (average solvent density is $\rho_s = 0.067\sigma^{-3}$). The figure only depicts the solvent particles (gray) and the grafted ends of the polymers (light blue). In this case, the solvent forms spherical droplets instead of elongated, cylindrical threads. We also note again that these solvent droplets are preferentially placed over areas where the grafting density is locally suppressed.

Experiments. For the experimental studies, we used polytBA brushes grafted to the surface of 160 nm thick PDMS films fabricated on the Si-wafer substrate. Soft elastic properties of PDMS provide opportunity to bring two polymer brushes into a dense contact while being immersed in a poor solvent—ethanol. Two identical brushes were pressed face-to-

DOI: 10.1021/acs.macromol.8b00865
Macromolecules XXXX, XXX, XXX−XXX

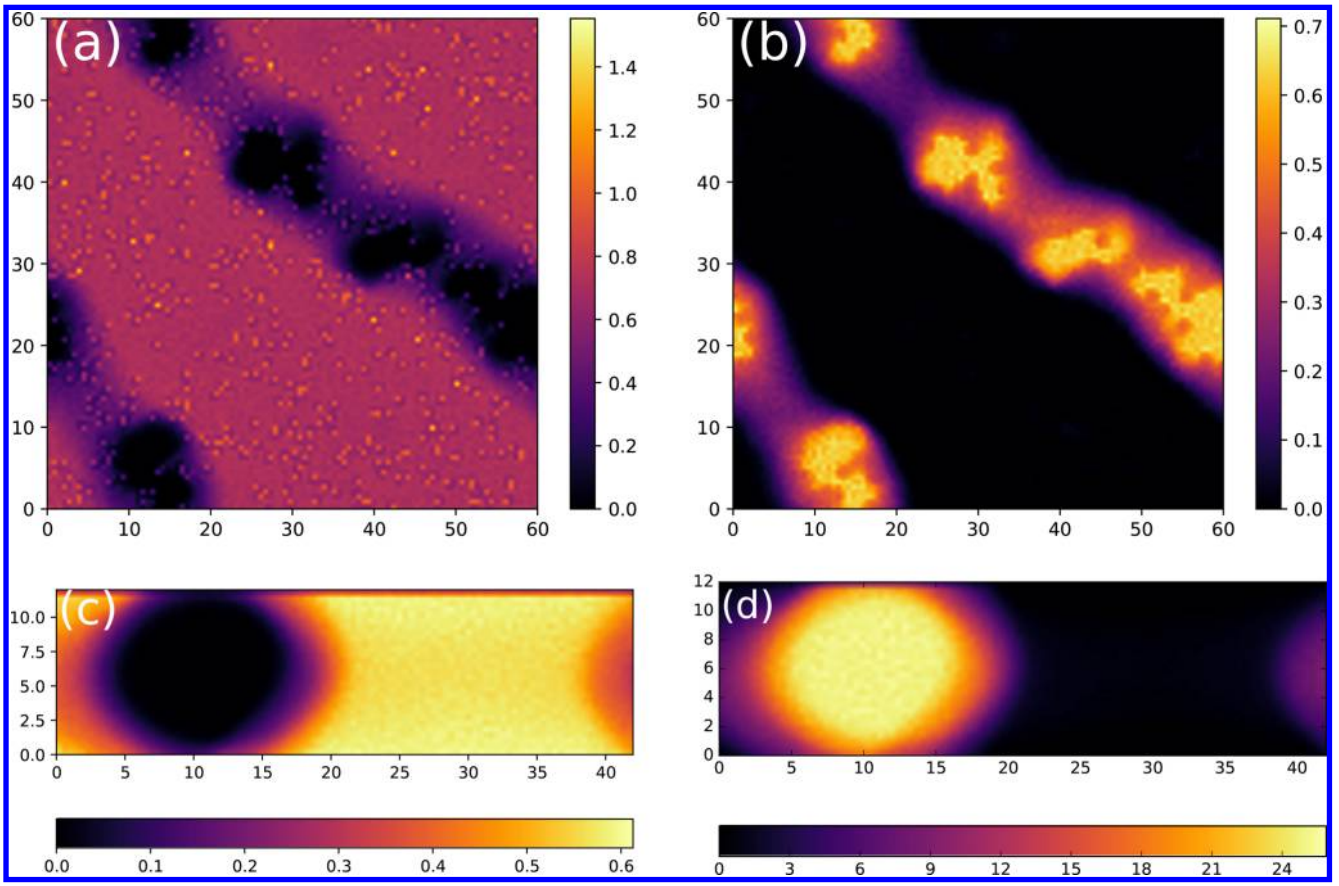

Figure 6. Number density of brush (a) and solvent particles (b) from a top-down perspective perpendicular to the grafting surfaces. $N_b = 32$ and $D = 19.3\sigma$. (c, d) Side views averaged along the axis of the solvent thread. The cylindrical geometry of the liquid thread and the concomitant deformation of the brush are clearly observed.

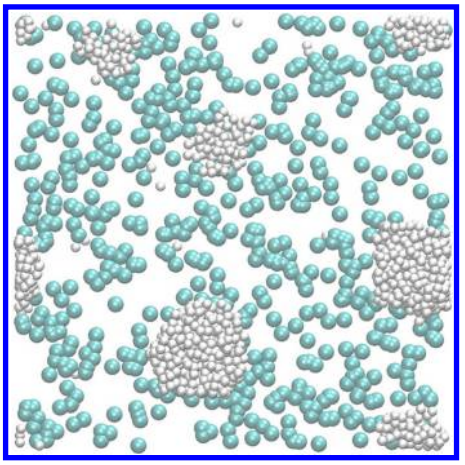

Figure 7. Configuration snapshot showing droplet formation of the solvent for a reduced solvent fraction. Only solvent particles and brush heads are shown, from a to top-down view. $N_b = 32$ and $D = 16\sigma$.

face to mimic conditions analyzed in the simulations. We immersed the samples in a bath filled with ethanol. Three samples of polymer brushes PtBA40, PtBA100, and PtBA190 with brush thicknesses of 40, 100, and 190 nm, respectively, and different grafting densities, as described in the Experimental Section, were studied in our experiments. Ethanol is a poor solvent for polytBA with the Flory–Huggins interaction parameter greater than 2 as was estimated based on the solubility parameters, 26.2 $MPa^{1/2}$ for ethanol and 16.4 $MPa^{1/2}$ for polytBA, respectively.[32] The topographical contrast was used to visualize brush morphologies prior and after apposing and compression of the brushes in the ethanol bath as shown in Figure 8. The characteristics lateral dimensions of the observed thread structures that appeared after compression scale with the brush thickness (see Figure 9).

A Simple Geometric Model. To rationalize the breaking up of the thin solvent layer between the two apposed polymer brushes upon compression, we use a simple geometric argument that is based on (i) the decrease in the contact area between solvent and brush and (ii) the impossibility to alter the average solvent fraction, $\bar{\phi}$, over a lateral length scale L that scales like R_e because of the irreversible grafting of the chain ends of the brush molecules.

We consider two morphologies as depicted in Figure 10: Panel a presents a sketch of the "sandwich" configuration brush–solvent–brush, when the solvent forms a thin layer of uniform thickness. $h_l = \bar{\phi}D$ and $h_b = \frac{1}{2}(D - h_l)$ denote the thickness of the solvent and brush layer, respectively. Assuming that the collapsed brush is not significantly stretched, i.e., $h_b \lesssim R_e$, the free energy per area, $\Delta F/A = 2\gamma$, is chiefly dictated by the polymer–solvent surface tension, γ.[a]

Panel b of Figure 10 illustrates the laterally segregated, solvent-thread structure, based on the two-dimensional profiles in Figure 6c,d. In the thread structure, we idealize the solvent domain as cylindrical with a radius, R, and L is the mean distance between two neighboring solvent threads. The solvent

DOI: 10.1021/acs.macromol.8b00865
Macromolecules XXXX, XXX, XXX–XXX

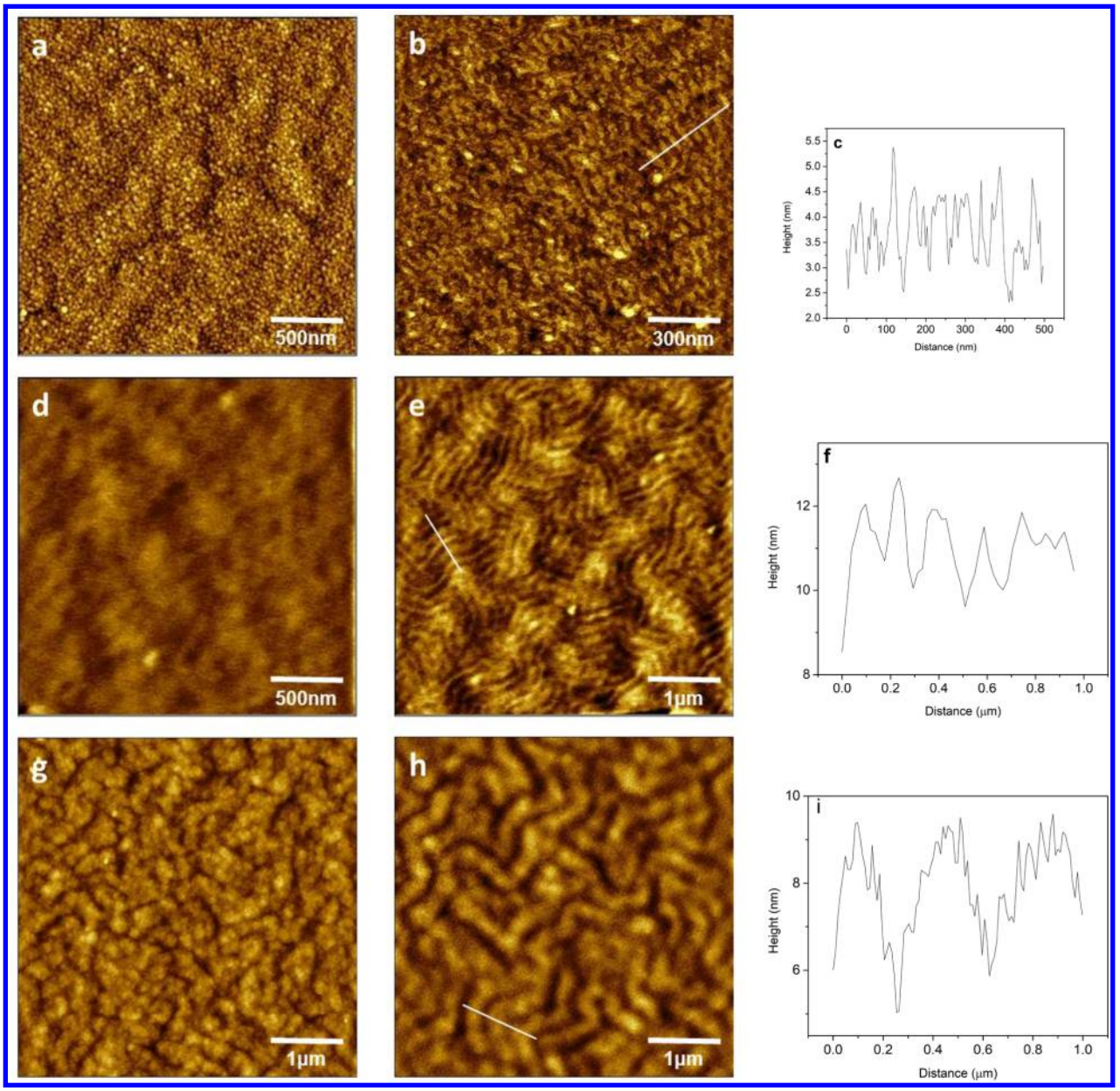

Figure 8. SPM topographical images (a, b, d, e, g, h) for polytBA brushes on PDMS substrates prior (a, d, g) and after the compression of the brushes (b, e, h) with corresponding cross-sectional profiles (c, f, i) for PtBA40 (a, b, c), PtBA100 (d, e, f), and PtBA190 (g, h, i). Straight lines on the images obtained after the compression mark locations of the cross-sectional profiles.

fraction can be written as $\bar{\phi} = \pi R^2/DL$, and the free energy takes the form

$$\frac{\Delta F}{A} = \frac{2\pi R\gamma}{L} = \frac{2\pi\gamma}{L}\sqrt{\frac{\bar{\phi}LD}{\pi}} \sim \frac{1}{\sqrt{L}} \tag{5}$$

According to eq 5, $\Delta F/A$ is minimal for large distances between cylinders L. In the following we explain why L cannot grow larger than order R_e. Assuming (i) a finite volume fraction, $\bar{\phi}$, of the solvent, (ii) a cylindrical shape of the solvent thread, $\bar{\phi} = \frac{\pi R^2}{LD}$ as well as $2R \leq D$ (cf. Figure 6), and (iii) a not highly stretched brush, $R_e \gtrsim h_b = (1 - \bar{\phi})D/2 \sim D$, we obtain $L = \frac{\pi R^2}{\bar{\phi}D} \leq \frac{\pi D}{4\bar{\phi}} \sim D \sim R_e$. The same argument can be generalized to spherical solvent domains (such as those shown in Figure 7). Altering the simple geometric consideration for the volume fraction, $\bar{\phi} = \frac{\frac{4\pi}{3}R^3}{DL^2}$, we obtain under the same assumptions $L^2 = \frac{4\pi}{3}\frac{R^3}{\bar{\phi}D} \leq \frac{\pi D^2}{6\bar{\phi}} \sim D^2 \sim {R_e}^2$. More generally, we note that the pattern formation gives rise to z-averaged, lateral composition variations, $\phi(x,y)$, that are characterized by a lateral length scale, L. Because the brush polymers are irreversibly grafted to the substrate, they are laterally immobile. Thus, the brush can only support lateral density variations on scales smaller than order R_e, and we expect that the condition $L \leq O(R_e)$ is independent from the details of the geometry of the solvent domains.

Let $D_{max}/2$ denote the maximal stable cylinder radius compatible with the brush deformation. The assumption of a circular cross section of the liquid threads requires that $D_{max} \leq$

DOI: 10.1021/acs.macromol.8b00865
Macromolecules XXXX, XXX, XXX−XXX

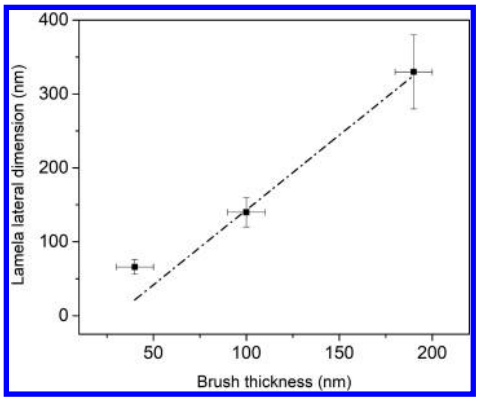

Figure 9. Dimensions of lateral structure vs the brush thickness. The dashed line is the linear fit with the Pearson correlation coefficient of 0.994.

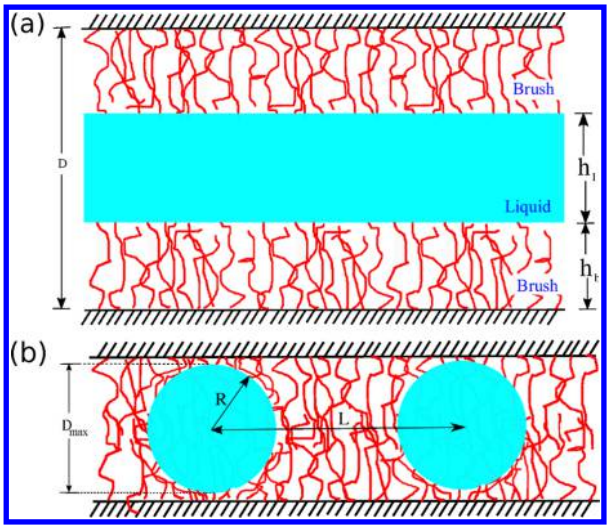

Figure 10. Sketch of geometric parameters for the sandwich configuration brush−liquid−brush (a) and the solvent−thread structure, which is represented locally by cylinders or droplets (b).

D and the irreversible grafting of the brush molecules yields the constraint ${D_{max}}^2/D = \frac{4}{\pi}\bar{\phi}L \sim L$. Thus, we obtain

$$\frac{\Delta F^*}{A} = \frac{\Delta F(R = D_{max}/2)}{A} = \frac{2\pi\gamma}{L}\frac{D_{max}}{2} \tag{6}$$

$$= \pi\gamma D_{max}\frac{4D\bar{\phi}}{\pi {D_{max}}^2} = 4\gamma\bar{\phi}\frac{D}{D_{max}} \tag{7}$$

Comparing the expressions of free energy for the "sandwich" configuration (a) and the solvent-thread configuration (b), the latter becomes stable for $\Delta F^*/A < 2\gamma$, or

$$2\gamma > \frac{\Delta F^*}{A} = 4\gamma\bar{\phi}\frac{D}{D_{max}} \tag{8}$$

i.e., solvent threads are formed for $\bar{\phi} < \frac{D_{max}}{2D}$ or $h_l < D_{max}/2$. At the onset of lateral structure formation, all length scales are of the same order of magnitude, $L = \pi\bar{\phi}D \sim h_b \lesssim R_e$, justifying the neglect of the entropic contribution to ΔF due to lateral stretching.

The nanopatterning relies on the existence of a polymer−solvent interface with a positive interface tension, $\gamma > 0$, but the predictions of our simple geometric model are independent of the specific magnitude of γ, and the transition solely depends on the geometric parameters and the solvent fraction, $\bar{\phi}$. This feature of the model arises from fact that we did not explicitly calculate the loss of conformational entropy as the chains laterally stretch but merely accounted for the changes of polymer conformations due to lateral pattern formation by the geometric constraint, $L \leq O(R_e)$. γ simply sets the scale of the free energy per area. At fixed $\bar{\phi}$, the transition from the sandwich to the solvent-thread structure occurs at $D \sim h_b$ and the characteristic lateral dimension also scales like $L \sim h_b$, in accord with the results of the simulations and experiments.

DISCUSSION AND CONCLUSIONS

In this work we have shown by computer simulations and experiments that two apposing planar polymer brushes compressing an incompatible liquid generate a lateral nanopatterning of the liquid, whose characteristic length is of the order of the brush thickness. The liquid compressed by the brushes forms interconnected liquid threads in the plane of the brush layers. We also developed a simple, geometric model to rationalize our findings. We argue that the phenomenon can be tailored to modify the liquid patterns by controlling the brush thickness.

The simulations also indicate that the lateral location of the liquid threads correlates with local reductions of the grafting density of the brush, whose chains are distributed randomly onto the substrate, in both typical experiments and simulations.

Additionally, we observed that if the amount of solvent is reduced, it is not enough to form a fingerprint-like pattern of liquid threads and nanoscale droplets are formed instead in regions of reduced grafting density. The effect is reminiscent, albeit different in geometry, of the known formation of dimples on a single brush exposed to a poor solvent liquid.[15−22]

We envision that the effect presented here is a reproducible, mechanically stable and versatile strategy for confining solvents on the nanoscale. Potentially, the effect could be used to fabricate nanopatterned systems, such as nanoparticles or nanoreactors. We hope that our study will stimulate further investigations along these directions.

AUTHOR INFORMATION

Corresponding Author

*E-mail: mmueller@theorie.physik.uni-goettingen.de (M.M.).

ORCID

Claudio Pastorino: 0000-0002-4833-5999
Sergiy Minko: 0000-0002-7747-9668
Marcus Müller: 0000-0002-7472-973X

Notes

The authors declare no competing financial interest.

ACKNOWLEDGMENTS

C.P. and M.M. thank the DFG under Grant SFB 937 A05 for financial support. C.P. additionally acknowledges financial support through Grants PIP 11220150100417 (CONICET), BAPIN 2017 (CNEA), PME 2015, and PICT-E 134-2014 (MINCYT). S.M. acknowledges the NSF Award CBET 1604526.

DOI: 10.1021/acs.macromol.8b00865
Macromolecules XXXX, XXX, XXX−XXX

■ ADDITIONAL NOTE

[a]We assume that grafting surface contributes in the two configurations equally.

■ REFERENCES

(1) Zoppe, J. O.; Ataman, N. C.; Mocny, P.; Wang, J.; Moraes, J.; Klok, H.-A. *Chem. Rev.* **2017**, *117*, 1105−1318.
(2) Azzaroni, O. *J. Polym. Sci., Part A: Polym. Chem.* **2012**, *50*, 3225−3258.
(3) Peng, S.; Bhushan, B. *RSC Adv.* **2012**, *2*, 8557−8578.
(4) Chen, T.; Ferris, R.; Zhang, J.; Ducker, R.; Zauscher, S. *Prog. Polym. Sci.* **2010**, *35*, 94−112.
(5) Stuart, M. A. C.; Huck, W. T. S.; Genzer, J.; Müller, M.; Ober, C.; Stamm, M.; Sukhorukov, G. B.; Szleifer, I.; Tsukruk, V. V.; Urban, M.; Winnik, F.; Zauscher, S.; Luzinov, I.; Minko, S. *Nat. Mater.* **2010**, *9*, 101−113.
(6) Barbey, R.; Lavanant, L.; Paripovic, D.; Schüwer, N.; Sugnaux, C.; Tugulu, S.; Klok, H.-A. *Chem. Rev.* **2009**, *109*, 5437−5527.
(7) Milner, S. T.; Witten, T. A.; Cates, M. E. *Macromolecules* **1988**, *21*, 2610−2619.
(8) Zhulina, Y. B.; Pryamitsyn, V. A.; Borison, O. V. *Vysokomol. Soedin., Ser. A* **1989**, *31*, 185−194.
(9) Murat, M.; Grest, G. S. *Macromolecules* **1989**, *22*, 4054−4059.
(10) Szleifer, I.; Carignano, M. A. *Adv. Chem. Phys.* **2007**, *94*, 165−260.
(11) Grest, G. S. *Adv. Polym. Sci.* **1999**, *138*, 149−183.
(12) Binder, K.; Milchev, A. *J. Polym. Sci., Part B: Polym. Phys.* **2012**, *50*, 1515−1555.
(13) Zhulina, E. B.; Borisov, O. V.; Pryamitsyn, V. A.; Birshtein, T. M. *Macromolecules* **1991**, *24*, 140−149.
(14) Grest, G. S.; Murat, M. *Macromolecules* **1993**, *26*, 3108−3117.
(15) Lai, P.; Binder, K. *J. Chem. Phys.* **1992**, *97*, 586.
(16) Williams, D. R. M. *J. Phys. II* **1993**, *3*, 1313−1318.
(17) Zhao, W.; Krausch, G.; Rafailovich, M.; Sokolov, J. *Macromolecules* **1994**, *27*, 2933.
(18) Zhulina, E. B.; Birshtein, T. M.; Priamitsyn, V. A.; Klushin, L. I. *Macromolecules* **1995**, *28*, 8612−8620.
(19) Singh, C.; Zhulina, E. B.; Gersappe, D.; Pickett, G. T.; Balazs, A. C. *Macromolecules* **1996**, *29*, 7637−7640.
(20) Koutsos, V.; van der Vegte, E. W.; Pelletier, E.; Stamouli, A.; Hadziioannou, G. *Macromolecules* **1997**, *30*, 4719−4726.
(21) Müller, M. *Phys. Rev. E: Stat. Phys., Plasmas, Fluids, Relat. Interdiscip. Top.* **2002**, *65*, 030802.
(22) Wenning, L.; Müller, M.; Binder, K. *Europhys. Lett.* **2005**, *71*, 639−645.
(23) Grest, G. S.; Kremer, K. *Phys. Rev. A: At., Mol., Opt. Phys.* **1986**, *33*, 3628−3631.
(24) Grest, G. S.; Lacasse, M. D.; Kremer, K.; Gupta, A. M. *J. Chem. Phys.* **1996**, *105*, 10583−10594.
(25) Pastorino, C.; Müller, M. *J. Chem. Phys.* **2014**, *140*, 166−174.
(26) Hoogerbrugge, P. J.; Koelman, J. M. V. A. *Europhys. Lett.* **1992**, *19*, 155.
(27) Soddemann, T.; Dünweg, B.; Kremer, K. *Phys. Rev. E: Stat. Phys., Plasmas, Fluids, Relat. Interdiscip. Top.* **2003**, *68*, 046702.
(28) Pastorino, C.; Kreer, T.; Müller, M.; Binder, K. *Phys. Rev. E* **2007**, *76*, 026706.
(29) Ionov, L.; Minko, S. *ACS Appl. Mater. Interfaces* **2012**, *4*, 483−489.
(30) Pastorino, C.; Binder, K.; Kreer, T.; Müller, M. *J. Chem. Phys.* **2006**, *124*, 064902.
(31) Pastorino, C.; Binder, K.; Müller, M. *Macromolecules* **2009**, *42*, 401−410.
(32) Aydin, S.; Erdogan, T.; Sakar, D.; Hizal, G.; Cankurtaran, O.; Tunca, U.; Karaman, F. *Eur. Polym. J.* **2008**, *44*, 2115−2122.

DOI: 10.1021/acs.macromol.8b00865
Macromolecules XXXX, XXX, XXX−XXX